



## RESEARCH ARTICLE

# In situ polymerized poly(acrylic acid)/alumina nanocomposites for Pb<sup>2+</sup> adsorption

Ya-Ping Wang<sup>1</sup>  | Peng Zhou<sup>1</sup> | Shi-Zhong Luo<sup>1</sup> | Sijie Guo<sup>2</sup> | Jing Lin<sup>3</sup> | Qian Shao<sup>4</sup> | Xingkui Guo<sup>4</sup> | Zhongqing Liu<sup>1</sup> | Jun Shen<sup>1</sup> | Bin Wang<sup>5</sup>  | Zhanhu Guo<sup>2</sup>

<sup>1</sup>School of Chemical Engineering, Sichuan University, Chengdu, Sichuan, China

<sup>2</sup>Integrated Composites Laboratory, Department of Chemical and Biomolecular Engineering, University of Tennessee, Knoxville, TN, USA

<sup>3</sup>School of Chemistry and Chemical Engineering, Guangzhou University, Guangdong, China

<sup>4</sup>College of Chemical and Environmental Engineering, Shandong University of Science and Technology, Qingdao, China

<sup>5</sup>Engineered Multifunctional Composites (EMC) Nanotech, Knoxville, TN, USA

## Correspondence

Shi-Zhong Luo, School of Chemical Engineering, Sichuan University, Chengdu, Sichuan, China.

Email: luosz@scu.edu.cn

Jing Lin, School of Chemistry and Chemical Engineering, Guangzhou University, Guangdong, China.

Email: linjing@gzhu.edu.cn

Bin Wang, Engineered Multifunctional Composites (EMC) Nanotech. LLC, Knoxville, TN, USA.

Email: bin\_wang@scu.edu.cn

Zhanhu Guo, Integrated Composites Laboratory, Department of Chemical and Biomolecular Engineering, University of Tennessee, Knoxville, TN, USA.

Email: zguo10@utk.edu

## Funding information

SINOPEC Maoming Company

## Abstract

In this study, two poly(acrylic acid)/alumina (PAA/alumina) nanocomposites with varied polymer loadings were prepared via in situ polymerization of preadsorbed acrylic acid. One composite would have a ~1/4-monolayer polymer coverage, while the other had a ~2-monolayer coverage. The produced composite materials were characterized in the adsorptive behavior of Pb<sup>2+</sup> from aqueous solution. When there was less PAA produced in a nanocomposite sample, there was higher Pb<sup>2+</sup> sorption capacity due to potentially less blocked alumina pores by in situ formed PAA. Isothermal and kinetic models for Pb<sup>2+</sup> sorption were applied by considering the effects of the initial Pb<sup>2+</sup> concentration and the contact time. The adsorption kinetics was best expressed using the pseudo-second-order equation. Through the isothermal studies, the maximum Pb<sup>2+</sup> monolayer adsorption capacity of 167.79 mg/g was recorded for the composite with higher PAA loading.

## KEYWORDS

alumina colloids, in situ polymerization, Pb<sup>2+</sup> sorption, poly(acrylic acid), polymer/inorganic nanocomposites

## 1 | INTRODUCTION

Polymer/inorganic nanocomposites are a family of materials that have received tremendous attentions lately because of their potential applications in biological sciences,<sup>[1]</sup>

nanotechnology,<sup>[2]</sup> optoelectronics,<sup>[3]</sup> therapeutics,<sup>[4]</sup> and catalysis.<sup>[5]</sup> These materials are not mere mixtures of inorganic phase and organic macromolecules. Instead, nanocomposites are able to coherently combine the unparalleled features of both the inorganic components and the organic

macromolecules.<sup>[6]</sup> Well-prepared nanocomposites preserve both the hardness and thermal stability of the inorganic skeleton, and the flexibility, ductility, dielectric properties, and processability of the organic polymers.<sup>[7]</sup>

Several methods are available for the preparation of polymer/inorganic nanocomposites, including impregnation, sol-gel, and in situ polymerization. Impregnation is a generic route to prepare composite materials which is very easy to process and takes short time to complete,<sup>[8]</sup> but the lack of control over the preparation process renders this method not suitable to synthesize materials with specifically fine-tuned physicochemical properties. The sol-gel route is highly effective to afford composite materials.<sup>[9]</sup> During the preparation, an inorganic or organometallic precursor in solution is hydrolyzed under control to form a submicron-size colloidal suspension (the sol). After catalysis with acid or base, a gel is subsequently produced. One disadvantage of this method is that the precursors are relatively limited or expensive compared to some widely used methods of preparing inorganic components.

The preparation of nanocomposites via in situ polymerization has shown a high level of control over the physicochemical properties of the products.<sup>[10]</sup> During in situ polymerization, monomeric precursors are adsorbed onto the inorganic phase first, followed by an often controlled polymerization process. The highly developed synthetic organic chemistry provides the in situ route advantages for producing composite materials with finely adjusted physicochemical characteristics. When preparing nanocomposites, using preexisting inorganic support ensures the preparation method more versatile with less product variation from batch to batch, but owing to the size restriction of polymers, nanocomposites produced with preexisting inorganic support via the impregnation route often have limited organic component incorporated inside the pores of the support. Using the in situ polymerization method, nanocomposites can be synthesized with high organic loadings because the small size of the monomers allows the organic molecules more fully penetrating the inorganic phase.<sup>[5]</sup> Another feature of the in situ polymerization method is that it is easier to modify the monomers with desired functionalities to afford specific characteristics in the products.

The large number of functional groups in organic polymers allows the nanocomposites a feasible candidate in applications for the metal ion removal from wastewater. In situ polymerization was carried out for the preparation of cross-linked PAA to form a network composed of chitosan and attapulgite.<sup>[11]</sup> This material showed higher efficacy in the removal of ammonium ions from wastewater than several reported adsorbents. Copolymerization of acrylic acid and acrylamide was employed to produce a 3D network microgel composed of fly ash and attapulgite.<sup>[12]</sup> This network demonstrated high adsorption capacity for  $\text{Pb}^{2+}$  in aqueous solution.

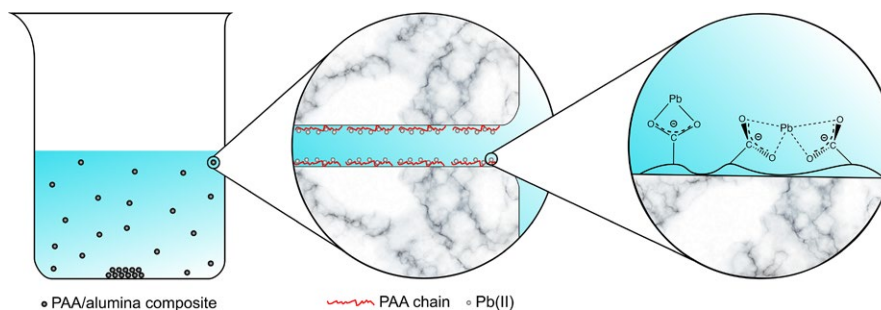
$\text{U}^{6+}$  ions were used as the template during the cross-linking of chitosan with glutaraldehyde in the presence of magnetite nanoparticles.<sup>[13]</sup> After removal of  $\text{U}^{6+}$  ions by acid bleaching, the composite material could be used as easily recyclable, reusable uranyl ion adsorbent. Dopamine (DA) was in situ polymerized on the surface of a hollow  $\text{Fe}_3\text{O}_4$  spherical template to obtain  $\text{Fe}_3\text{O}_4/\text{PDA}$  dual-shelled microspheres, and the as-prepared materials held a faster adsorption dynamic process and a higher adsorption capacity for  $\text{Eu}(\text{III})$  entrapment.<sup>[14]</sup>

Fine-tune-prepared inorganic/polymer nanocomposites maintain a high degree of specific surface area of the metal oxide skeleton and myriad interactive sites of functional groups of the macromolecules. The synergistic effects of high surface area of the inorganic phase and the coordination capability of the polymers make the metal ion sorptivity of the composite materials superior to that of either pristine metal oxides or polymers. When the nanocomposites were prepared using the impregnation approach, the inorganic skeleton pore size restricted the sorption of macromolecules into the composite material.<sup>[15]</sup> We fabricated PAA/alumina nanocomposites by in situ polymerization of acrylic acid to afford composite materials with high PAA content (Y.-P. Wang, P. Zhou, S.-Z. Luo, J. Shen, B. Wang, X.-P. Liao, Z. Guo, unpublished data).<sup>[16]</sup> The produced hybrid materials demonstrated high  $\text{Pb}^{2+}$  ion sorptivity. In this study, we systematically investigate the  $\text{Pb}^{2+}$  sorption properties of the PAA/alumina produced by the in situ polymerization route. The results are also compared with the simultaneously conducted research in which the  $\text{Pb}^{2+}$  sorption experiments were carried out on PAA/alumina nanocomposites prepared via the impregnation process (P. Zhou, Y.-P. Wang, S.-Z. Luo, B. Wang, P. Bernazzani, T. M. Nguyen, unpublished data).

## 2 | EXPERIMENTS AND METHODS

### 2.1 | Materials

Acrylic acid was acquired from Chengdu Kelong Chemical Co. 4,4'-Azobis(4-cyanovaleric acid) (V501) was purchased from Chengdu Best Chemicals Co. Ltd. Poly(acrylic acid) with  $M_w$  800–1,000 was purchased from Tianjin Kemiou Chemicals Co. in 30% solution. Poly(acrylic acid) with  $M_w$  3,000 was acquired from Shanghai Aladdin Reagents Co. in 50% solution. Poly(acrylic acid) with  $M_w$  100,000 was supplied by Sigma-Aldrich (Shanghai) in 35% solution.  $\gamma$ -Alumina was obtained from Tianjin Kemiou Chemicals Co., and its ground powders in 40–60 mesh range were activated at 500°C for 3 hr prior to use. Other reagents were of analytical grade. Deionized water was used with a conductivity of  $\leq 1.0 \mu\text{S/m}$ . All reagents were used as received without further purification unless stated otherwise.



**SCHEME 1** Illustration of  $\text{Pb}^{2+}$  adsorption process

## 2.2 | Preparation of PAA/alumina composite samples

The preparation of PAA/alumina composites followed our previous report.<sup>[16]</sup> Briefly, 5.0 g of activated alumina was added with 2.0 ml of acrylic acid ethanol solution (10% or 90%) and setting for 1 hr. The acrylic acid-loaded alumina was added with the chain transfer agent (CTA) and V501 (both in 50% NaOH solution). The amounts of the two reagents were calculated according to the adsorbed acrylic acid (determined via thermogravimetry): AA:CTA:V501 = 40:1:0.1 in molar ratios. The mixture was added with water (20 ml), stirred at 65°C for 8 hr, and quenched with ice water. The mixture was then adjusted to pH 5.0–5.5 using NaOH, filtered and rinsed repeatedly, and dried at 60°C for 10 hr. The prepared samples were labeled  $\text{P}_{10,\text{in}}/\text{Al}$  and  $\text{P}_{90,\text{in}}/\text{Al}$ , respectively, based on the acrylic acid loading of each sample.

## 2.3 | Solution properties of alumina, PAA, and PAA/alumina composites

A batch equilibrium procedure was employed to determine several solution properties of alumina, PAA, and PAA/alumina composite samples. The point of zero charge (PZC) of alumina was measured using either the mass titration or immersion method. In the mass titration method,<sup>[17]</sup> batches of alumina powders were placed in flasks and added with water to make suspensions of various alumina concentrations. The ionic strength of the suspensions was adjusted to 0.01 M by the addition of  $\text{NaNO}_3$ . After setting for 48 hr, the equilibrium pH value of each supernatant was measured and plotted against the concentration of the corresponding suspension. In the immersion technique,<sup>[18]</sup> alumina powder was placed in flasks and added with  $\text{NaNO}_3$  solution of different pH. A blank at each pH value without alumina was also prepared. After setting for 48 hr, the pH values of both the supernatants and blanks were measured.

The dissociation constants of both PAA and the two composite materials  $\text{P}_{10,\text{in}}/\text{Al}$  and  $\text{P}_{90,\text{in}}/\text{Al}$  were measured. A certain amount of sample based on PAA content was dispersed with ~5 ml water. An aliquot of 0.20 ml of 0.025 M NaOH was titrated into the dispersion under swirling. After

equilibration time, the pH value of the dispersion was recorded.

The metal ion sorption properties of the composites were reported as the average of triplicate measurements. In a typical experiment, an aliquot of  $\text{Pb}^{2+}$  solution (25 ml) was added with PAA/alumina nanocomposites (0.01 g), standing for appropriate time periods and filtered (see Scheme 1). Lead content of the supernatant was directly analyzed with atomic absorption spectrophotometry (AAS) (AA32DCRT; Shanghai Analytical Instrument Co.). Aqueous lead standard solutions were prepared from  $\text{Pb}(\text{NO}_3)_2$  solution of pH 5.0–5.1 to obtain standards for AAS. When the lead content of a solid was to be determined, the solid was dissolved with 50% phosphoric acid, diluted with water, and analyzed with AAS. The lead sorption kinetics was analyzed by filtering the sorption solution at different time intervals and measuring the Pb content of the supernatant. The effect of  $\text{Pb}^{2+}$  concentration on sorption amount was tested in  $\text{Pb}(\text{NO}_3)_2$  solutions of pH 5.0–5.1.

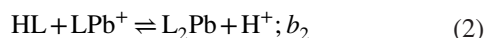
## 2.4 | Characterizations

The morphologies of the samples were determined using a JEOL JSM-7500F field emission scanning electron microscope (SEM), operated at 15 kV. Thermogravimetry (TG) (HCT-2 Differential Thermal Balance; Beijing Hengjiu Scientific Instrument Co.) was operated in the range of 80–700°C in air. The sample was initially heated to 80°C for 20 min to remove atmospheric water. The process was monitored until the weight variation reached a level of  $\leq 0.01$  mg. The sample was then heated at a heating rate of 10°C/min, except the halt for 10 min at 450°C for the complete decomposition of PAA chains. The specific surface area, total pore volume, and average pore diameter were determined from the nitrogen adsorption–desorption isotherms at  $-196^\circ\text{C}$ , which were measured using an automated surface area and pore size analyzer (Quadrastorb SI apparatus). Before each measurement, the samples were degassed in vacuum at 120°C for 3 hr. Specific surface area of samples was calculated using the Brunauer–Emmett–Teller (BET) method, and the pore size distribution and average pore diameter were determined according to the

Barrett–Joyner–Halenda (BJH) method applied to desorption isotherms.

## 2.5 | Complexation equilibrium constant calculation

We use the modified Bjerrum model to investigate the complexation equilibrium of PAA and  $\text{Pb}^{2+}$  ions.<sup>[19]</sup> The serial formation of PAA– $\text{Pb}^{2+}$  complexes can be expressed in the following equations:



Here, L represents the PAA carboxylate, and serial stability constants  $b_1$  and  $b_2$  are given by the following equations:

$$b_1 = \frac{[\text{LPb}^+][\text{H}^+]}{[\text{HL}][\text{Pb}^{2+}]} \quad (3)$$

$$b_2 = \frac{[\text{L}_2\text{Pb}][\text{H}^+]}{[\text{HL}][\text{LPb}^+]} \quad (4)$$

We assume that except the protonation of  $\text{LPb}^+$  and  $\text{L}_2\text{Pb}$  complexes, the ligand sites on PAA coordinating with  $\text{Pb}^{2+}$  are more than one. The complex  $\text{L}_2\text{Pb}(\text{HL})_n$  formed via a nonprotonated process is shown as follows:



The equilibrium constant  $k_3$  is determined by the following equation:

$$k_3 = \frac{[\text{L}_2\text{Pb}(\text{HL})_n]}{[\text{L}_2\text{Pb}][\text{HL}]^n} \quad (6)$$

So the total  $\text{Pb}^{2+}$  concentration coordinated with PAA  $[M_p]$  and the total PAA concentration  $[P_t]$  are given by the following equations:

$$\begin{aligned} [M_p] = & b_1[\text{Pb}^{2+}] \frac{[\text{HL}]}{[\text{H}^+]} + b_1 b_2 [\text{Pb}^{2+}] \left\{ \frac{[\text{HL}]}{[\text{H}^+]} \right\}^2 \\ & + b_1 b_2 k_3 [\text{Pb}^{2+}] \left\{ \frac{[\text{HL}]}{[\text{H}^+]} \right\}^2 [\text{HL}]^n \end{aligned} \quad (7)$$

$$\begin{aligned} [P_t] = & \left\{ 1 + \left( \frac{K_a}{[\text{H}^+]} \right)^{1/\beta} \right\} [\text{HL}] + b_1 [\text{Pb}^{2+}] \frac{[\text{HL}]}{[\text{H}^+]} \\ & + 2b_1 b_2 [\text{Pb}^{2+}] \left\{ \frac{[\text{HL}]}{[\text{H}^+]} \right\}^2 + (2+n)b_1 b_2 k_3 [\text{Pb}^{2+}] \\ & \left\{ \frac{[\text{HL}]}{[\text{H}^+]} \right\}^2 [\text{HL}]^n \end{aligned} \quad (8)$$

Under experimental conditions,  $[P_t]$  and  $[\text{H}^+]$  are known. After the values of  $b_1$ ,  $b_2$ ,  $k_3$ , and  $n$  are obtained, the coordination quantity of PAA to  $\text{Pb}^{2+}$  ( $q$ ) can be calculated using the solution  $[\text{Pb}^{2+}]$  via the following equation:

$$q = \frac{[M_p]}{[P_t]} = f \{ [\text{Pb}^{2+}]; b_1, b_2, k_3, n \} \quad (9)$$

Equation (9) can be calculated via nonlinear regression and expressed as a plot.

## 2.6 | Desorption and reuse after desorption

After adsorbing  $\text{Pb}^{2+}$  ions,  $\text{P}_{90,\text{in}}/\text{Al}$  (0.01 g) was separated by centrifuging and dried at  $60^\circ\text{C}$ . Then, the sample was left in contact with 25 ml 1 M  $\text{HNO}_3$ . After holding still at room temperature for 4 hr, the  $\text{Pb}^{2+}$  concentration of supernatant was analyzed via the same method as before. The  $\text{P}_{90,\text{in}}/\text{Al}$  after desorption was reused in adsorption experiment, and the adsorption–desorption was repeated five times.

## 3 | RESULTS AND DISCUSSION

### 3.1 | Characterization of PAA/alumina, alumina, and PAA

The preparation of PAA/alumina nanocomposites and the determination of  $\text{Pb}^{2+}$  adsorption properties were elaborately described in our previous study.<sup>[16]</sup> In that study, PAA/alumina composites with varied PAA loadings were prepared through the in situ polymerization of acrylic acid. The formation of such composite materials was confirmed using FTIR, TG,  $\text{N}_2$  adsorption–desorption, and solution titration. In the current study, more material properties of the PAA/alumina nanocomposites were analyzed, especially those associated with the metal ion sorption behavior.

Here, we select two such samples,  $\text{P}_{10,\text{in}}/\text{Al}$  and  $\text{P}_{90,\text{in}}/\text{Al}$ , as representatives of the PAA/alumina composite materials prepared via the in situ polymerization route.<sup>[16]</sup> The scanning electron microscopy (SEM) images of pristine alumina,  $\text{P}_{10,\text{in}}/\text{Al}$ , and  $\text{P}_{90,\text{in}}/\text{Al}$  are displayed in Figure 1. No obvious difference is observed among the three samples, and there is no distinction whether PAA covered the alumina surface in the two composite samples. This observation is consistent with our previous SEM results of PAA/alumina samples prepared via impregnation.<sup>[15]</sup> Incorporation of alumina with PAA, either through impregnation or through in situ polymerization, does not alter the oxide microstructure at the SEM-observable scale.

The amounts of PAA adsorbed on alumina were analyzed using TG (Figure 2). Sample  $\text{P}_{10,\text{in}}/\text{Al}$  had a PAA adsorption amount of  $99.11 \mu\text{g}/\text{m}^2$  on the (inner pore)

surface of alumina, equivalent to a  $\sim 1/4$ -monolayer coverage. Sample  $P_{90,\text{in}}/\text{Al}$  had a PAA adsorption amount of  $749.80 \mu\text{g}/\text{m}^2$ , about a two-monolayer coverage. We can further elaborate the PAA adsorption characteristics of the two samples by comparison with samples prepared via the impregnation method, in which PAA/alumina samples were produced by employing PAA with different  $M_w$  (P. Zhou, Y.-P. Wang, S.-Z. Luo, B. Wang, P. Bernazzani, T. M. Nguyen, unpublished data). Among the impregnation-prepared samples, composites  $H_{1k}$  and  $H_{3k}$ , prepared from 0.003 M immersion solutions of PAA with  $M_w$  of 800–1,000 and 3,000, respectively, showed an adsorption amount close to that of  $P_{10,\text{in}}/\text{Al}$ . In both  $H_{1k}$  and  $H_{3k}$ , PAA infiltration of alumina is considered the main mechanism of polymer adsorption. With higher PAA immersion solution concentration, the PAA adsorption amounts increased for both  $H_{1k}$  and  $H_{3k}$ , but only to the level of slightly over one monolayer. On the other hand,  $H_{100k}$  prepared from PAA with a  $M_w$  of 100,000 reached polymer adsorption amounts in the range of  $964.8\text{--}1,011 \mu\text{g}/\text{m}^2$ , depending on the initial PAA concentration. PAA with  $M_w$  of 100,000 is incapable to infiltrate alumina pores; therefore, the PAA adsorption value of  $749.80 \mu\text{g}/\text{m}^2$  in  $P_{90,\text{in}}/\text{Al}$  would contain considerable portion on the outside surface of alumina.

To test the stability of the nanocomposites in solution, we used the Soxhlet extraction to extract the composite materials with water vapor for 72 hr. The desorption curves along with the samples without extraction are depicted in Figure 2.

It can be observed that the amount of desorbed PAA is less in  $P_{10,\text{in}}/\text{Al}$  (about 7%) than in  $P_{90,\text{in}}/\text{Al}$  (about 28%). In  $P_{10,\text{in}}/\text{Al}$ , most PAA resided inside the alumina pores, so the polymers would encounter large diffusion resistance during extraction. In  $P_{90,\text{in}}/\text{Al}$ , there was partial distribution of PAA on the outer surface of alumina which could be easily removed from the oxide. In general, both samples showed relatively low PAA desorption, indicating a good stability of the produced composite materials.

The PZC value of a metal oxide can provide information on the adsorption potential of the colloid toward certain solutes. The PZC of alumina was detected to better understand the solution properties of the PAA/alumina nanocomposites. Here, we apply both the mass titration method and the immersion method. In the mass titration experiment, a series of alumina suspensions with concentrations of 0.01%, 0.1%, 1%, 5%, 10%, and 20% were prepared and added with  $\text{NaNO}_3$  to obtain a solution ionic strength of 0.01 M. After standing for 48 hr, the supernatant of each suspension was separated and the pH value was measured (Figure 3a). The plot shows that at high suspension concentrations, a plateau would be reached which was the PZC of the oxide. The PZC value determined for  $\gamma\text{-Al}_2\text{O}_3$  is 9.00.

In the immersion experiment, a series of alumina suspensions of 0.01 M ionic strength were adjusted to pH 8.0, 8.5, 9.0, 9.5, and 10.0, respectively, with an error range of  $\pm 0.02$ . A blank solution series with no alumina powders were prepared in the same fashion. After standing for 48 hr, the supernatant of each suspension was separated. The pH of the

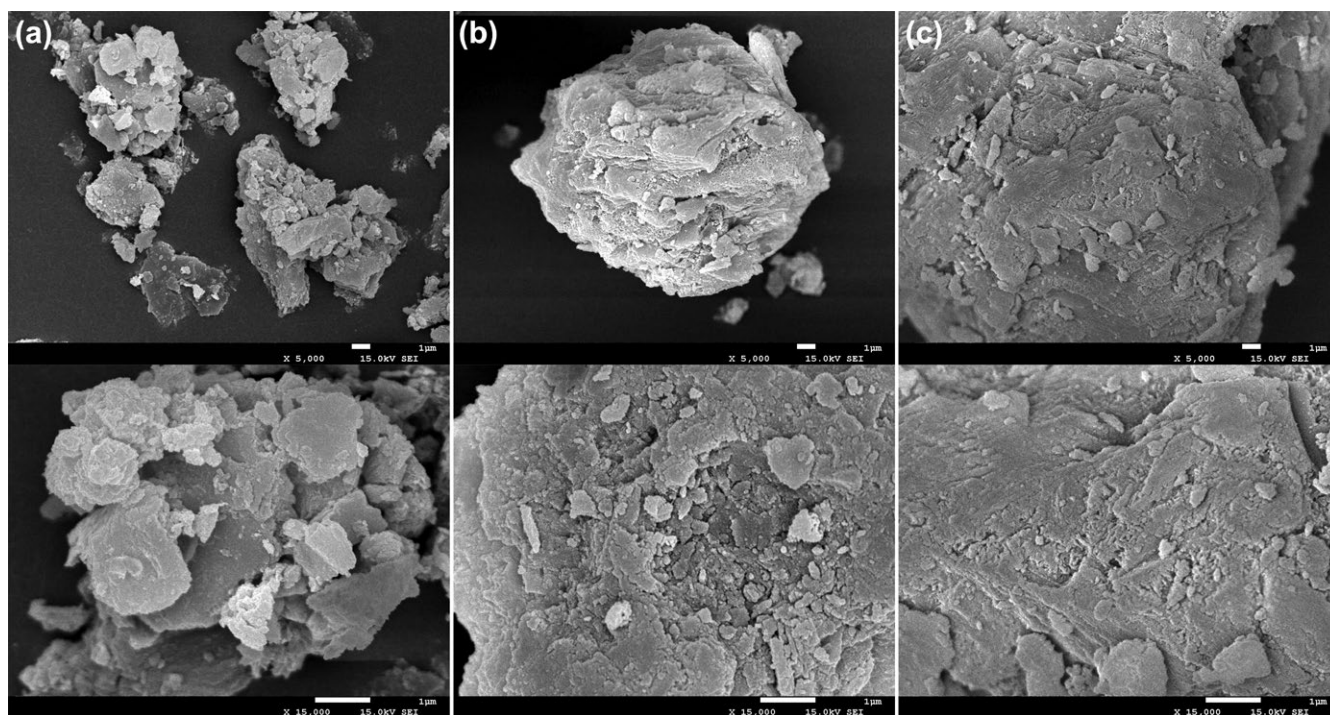


**FIGURE 1** Surface morphologies of (a) pristine alumina, (b)  $P_{10,\text{in}}/\text{Al}$ , and (c)  $P_{90,\text{in}}/\text{Al}$

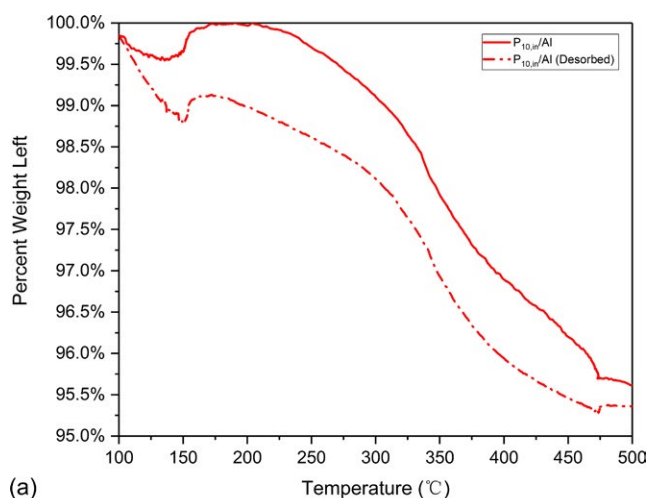
suspension and the corresponding blank was measured. The pH changes during the equilibrium were calculated according Equation (10):

$$\Delta\text{pH} = \text{pH}_{\text{blank}} - \text{pH}_{\text{sus}} \quad (10)$$

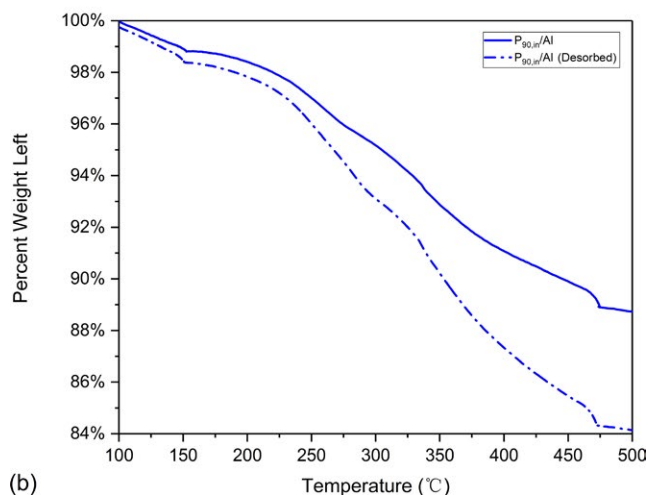
Here,  $\text{pH}_{\text{blank}}$  was the pH value of a blank, and  $\text{pH}_{\text{sus}}$  was the pH value of the corresponding suspension. Plotting  $|\Delta\text{pH}|$  versus the final pH generated a diagram, in which the final pH 8.81 corresponding to the minimum  $|\Delta\text{pH}|$  value was the PZC of the colloid, as observed in Figure 3b. The PZC values determined using both the mass titration method and the immersion method are close to the values determined in the literature report.<sup>[18]</sup> At  $\text{pH} < 8.81$  (the lower of the two),  $\gamma\text{-Al}_2\text{O}_3$  surface would present positive charges. The positive charge of alumina surface is beneficial for the adsorption of ionized PAA molecules.

The dissociation constants of PAA,  $\text{P}_{10,\text{in}}/\text{Al}$ , and  $\text{P}_{90,\text{in}}/\text{Al}$  were determined by the pH titration method.<sup>[16]</sup> The  $\text{p}K_a$  and

$\beta$  values of the two composites and those of three commercial PAA samples are listed in Table 1. From the table, the  $\text{p}K_a$  values of the commercial PAA samples are close to 6.5, a value reported in the literature.<sup>[20]</sup> When the solution ionic

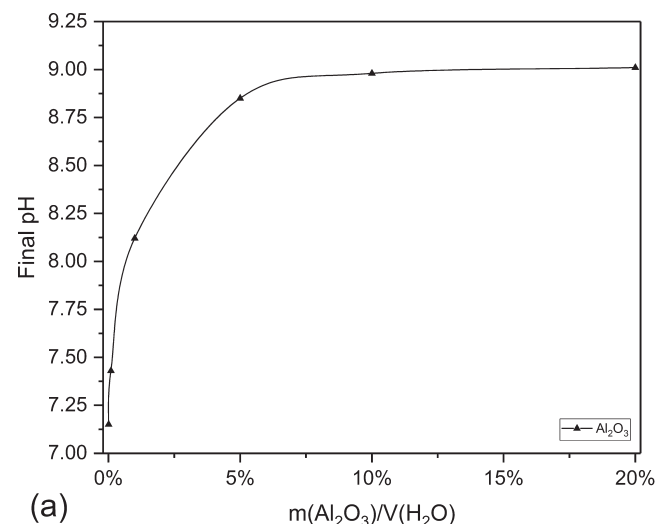


(a)

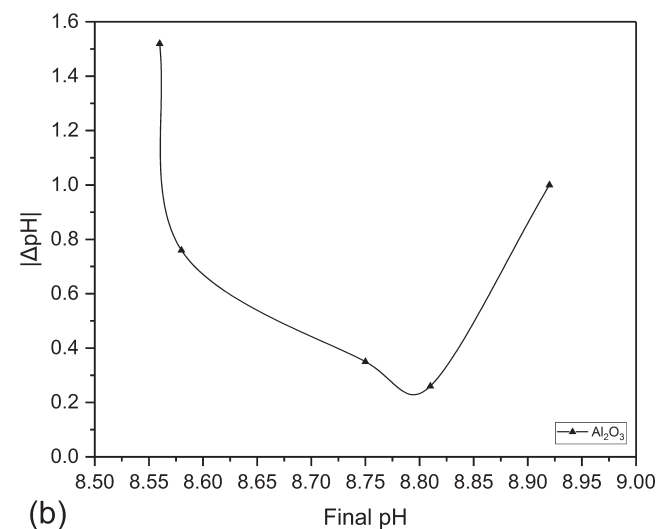


(b)

**FIGURE 2** TG traits of PAA/alumina composites (a) before and (b) after desorption of PAA



(a)



(b)

**FIGURE 3** Plots of (a) final pH vs alumina concentration measured by mass titration and (b)  $|\Delta\text{pH}|$  vs final pH values by immersion techniques

**TABLE 1** Dissociation constants of PAA/ $\gamma\text{-Al}_2\text{O}_3$  composites and some commercial PAA samples with various molecular weights

|                                     | $\beta$ | $K_a$                 | $\text{p}K_a$ | $R^2$ |
|-------------------------------------|---------|-----------------------|---------------|-------|
| $\text{P}_{10,\text{in}}/\text{Al}$ | 1.697   | $6.42 \times 10^{-7}$ | 6.192         | .999  |
| $\text{P}_{90,\text{in}}/\text{Al}$ | 1.265   | $2.33 \times 10^{-6}$ | 5.632         | .999  |
| PAA ( $M_w$ 800)                    | 2.829   | $8.83 \times 10^{-7}$ | 6.054         | .999  |
| PAA ( $M_w$ 3,000)                  | 2.478   | $1.20 \times 10^{-7}$ | 6.920         | .999  |
| PAA ( $M_w$ 100,000)                | 2.477   | $3.06 \times 10^{-7}$ | 6.514         | .999  |

**TABLE 2** Comparison of  $\text{Pb}^{2+}$  adsorption amounts of different alumina-based composites

| Adsorbent   | $q_{\max}$ (mg/g)  | $q_e$ (mg/g)       | Experimental condition   | Ref  |
|---|--------------------|--------------------|--|--|
| Planar $\gamma\text{-Al}_2\text{O}_3$                 |                    | 5.38 <sup>a</sup>  | pH 6.00, $I$ 0.01 M, $c_0$ 3.536 mg/L, $\Gamma_{\max}$ 0.26 $\mu\text{mol}/\text{m}^2$ , $t$ 24 hr | [25]   |
| Synthesized $\gamma\text{-Al}_2\text{O}_3$            | 7.39               |                    |  | [26]   |
| P(AMPSG/AAC/NVP/HEMA)                                 | 22.73 <sup>a</sup> |                    | $c_0$ 100–3,000 mg/L, $t$ 24 hr  | [27]   |
| $\gamma\text{-Al}_2\text{O}_3$                        |                    | 25.90 <sup>a</sup> | pH 6.50, $I$ 0.1 M, $c_0$ 0.414 mg/L, SSA 100 $\text{m}^2/\text{g}$ , $t$ 500 hr                   | [28]   |
| PAA/ $\text{Al}_2\text{O}_3$ -TPPM                    |                    | 28.00 <sup>a</sup> | pH 5.00, $c_0$ 150 mg/L, $t$ 24 hr   | [29]   |
| Activated $\text{Al}_2\text{O}_3$                     | 83.33              |                    | $c_0$ 10–100 mg/L, $t$ 2 hr  | [30]   |
| PAA/ $\text{Al}_2\text{O}_3$ (impregnation)           |                    | 71.45              | pH 5.00, $c_0$ 60 mg/L, $t$ 1 hr   | P. Zhou, Y.-P. Wang, S.-Z. Luo, B. Wang, P. Bernazzani, T. M. Nguyen, unpublished data |
| PAA/ $\text{Al}_2\text{O}_3$ (in situ polymerization) |                    | 86.98              | pH 5.00, $c_0$ 60 mg/L, $t$ 1 hr   | This work  |

<sup>a</sup>Estimated from the data present in the literature.

strength  $I$  is high,  $\text{p}K_a$  can present a lower value.<sup>[21]</sup> The two composite samples have an average  $\text{p}K_a$  value slightly lower than that of the three commercial PAA samples. This implies that adsorption on alumina surface causes PAA molecules more prone to dissociate. In other words, adsorption on alumina makes PAA molecules slightly more acidic. Between the two composite samples, the more the ratio of the alumina ( $\text{P}_{10,\text{in}}/\text{Al}$ ), the higher the  $\text{p}K_a$  of the material; and sample  $\text{P}_{10,\text{in}}/\text{Al}$  has a higher  $\beta$  value than  $\text{P}_{90,\text{in}}/\text{Al}$ , indicating less carboxylic acid amount per material mass.

### 3.2 | $\text{Pb}^{2+}$ adsorption on PAA/alumina nanocomposites

One foremost property of the PAA/alumina composite materials is their metal ion sorption behavior. Solution pH has a significant effect on the metal ion sorption results of these materials.<sup>[22]</sup> It is generally accepted that the carboxylic acid groups are considered the predominant metal ion sorption sites. Metal ions may be adsorbed onto the composites through ion exchange with  $-\text{COOH}$ , or complexation with  $-\text{COO}^-$ .<sup>[23]</sup> On the other hand, the stability constant of  $\text{Pb}^{2+}$ -PAA (6.75–7.0) is higher than that of  $\text{Pb}^{2+}$ -alumina (6.0), but there exist enough strong-adsorbing sites on alumina for metal ion to bind.<sup>[24]</sup>

Lead sorption on pristine alumina and PAA/alumina samples was performed in a batch equilibrium procedure. In a typical experiment, an aliquot of  $\text{Pb}^{2+}$  solution of 25 ml was added with the adsorbent ( $0.01 \pm 0.0002$  g), standing for various time periods, and filtered. Examination of the adsorption curves (not shown here) of pristine alumina,  $\text{P}_{10,\text{in}}/\text{Al}$ , and  $\text{P}_{90,\text{in}}/\text{Al}$  reveals that the three samples behaved highly similarly toward lead sorption.<sup>[16]</sup> The adsorption of composite

reached a plateau after  $\sim 30$  min, attributed to the large quantities of carboxylic acid groups present in the samples. It is suggested that PAA directly attached to alumina surface contributed significantly to lead ion sorption.

The lead ion sorption behavior of the PAA/alumina nanocomposites is compared to that of some alumina-based materials reported in the literature<sup>[25–30]</sup> (Table 2). It is obvious that the PAA/alumina nanocomposites prepared in our studies had very high lead ion sorptivities. The composite materials produced via in situ polymerization held more lead than that prepared via the impregnation method. In the PAA/alumina composite materials, the lead sorptivity is dependent on the initial  $\text{Pb}^{2+}$  concentration.<sup>[16]</sup> Higher initial  $\text{Pb}^{2+}$  concentrations

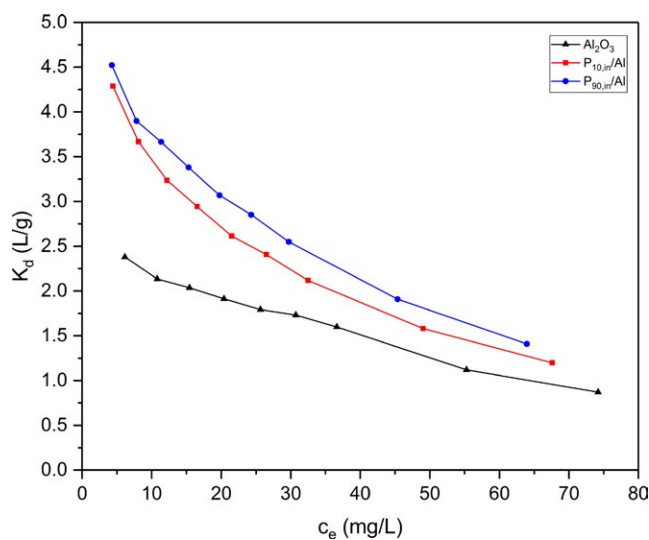


**FIGURE 4** Relationship between distribution coefficient ( $K_d$ ) and initial  $\text{Pb}^{2+}$  concentration

lead to higher lead sorptivity. It is suggested that the lead ion adsorption is an equilibrium process in which the high  $\text{Pb}^{2+}$  concentrations provide strong driving forces for lead diffusion. Here, we use the concept of distribution coefficient  $K_d$  (L/g) to describe the effect of initial  $\text{Pb}^{2+}$  concentration on sorptivity.  $K_d$  is calculated according to the following equation:<sup>[31]</sup>

$$K_d = \frac{(c_0 - c_e)V}{c_e m} \quad (11)$$

The  $K_d$  values were plotted against  $c_e$  after they were acquired (Figure 4). It is observed that  $K_d$  value decreases with increasing initial  $\text{Pb}^{2+}$  concentration. At high initial  $\text{Pb}^{2+}$  concentrations, the adsorbing sites of the adsorbent materials were saturated quickly, so more  $\text{Pb}^{2+}$  ions stayed in solution as free ions. Therefore, at low metal ion/adsorbent ratios,  $\text{Pb}^{2+}$  adsorption takes place at the high-energy sites. With the gradual occupation of the high-energy sites by  $\text{Pb}^{2+}$  ions upon increasing the metal ion/adsorbent ratio, the adsorption shifts to the sites with lower energies. This shift causes the lowering of adsorption efficiency.<sup>[30]</sup>

The effect of the solution pH on  $\text{Pb}^{2+}$  adsorption is illustrated in Figure 5, in which the results of triplicate trials are displaced with error bars. The solution pH range of 4–6 was selected because  $\text{Pb}^{2+}$  ions tend to precipitate at  $\text{pH} > 6$ .<sup>[30]</sup> From the figure, the  $\text{Pb}^{2+}$  adsorption capacity of PAA/alumina composites enhances slowly with increasing solution pH, while that of pristine alumina rapidly increases until reaching a plateau. The effect of solution pH on adsorption capacity can be interpreted in terms of the interaction between the adsorption active sites and solution  $\text{Pb}^{2+}$  ions. Under low solution pH, there is a

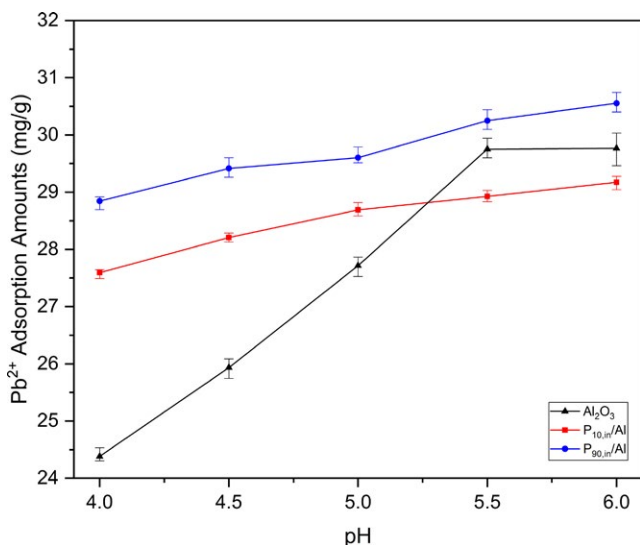


**FIGURE 5** Influence of pH values on  $\text{Pb}^{2+}$  adsorption in alumina and PAA/alumina composites

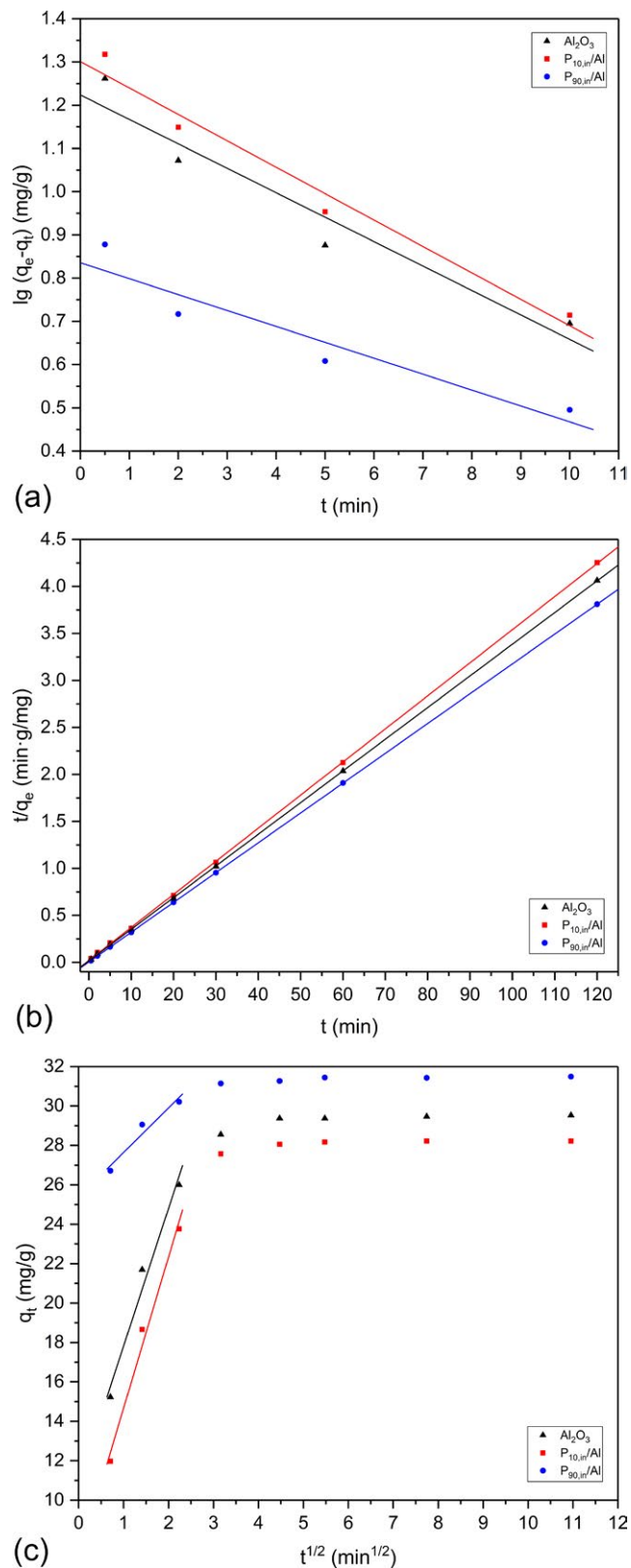


**FIGURE 6** Fitted plots of (a) pseudo-first-order model, (b) pseudo-second-order model, and (c) intra-particle diffusion model of  $\text{Pb}^{2+}$  adsorption in alumina and PAA/alumina composites



smaller portion of PAA molecules being ionized, and the hydrated proton  $\text{H}_3\text{O}^+$  binds more tightly to the active sites of PAA molecules to repel attraction of  $\text{Pb}^{2+}$  ions.<sup>[32]</sup> With higher solution pH, the ionization degree of PAA increases that offers more binding sites for  $\text{Pb}^{2+}$  ion complexation. Even the free lone pairs on  $-\text{OH}$  and  $-\text{COOH}$  start to attract  $\text{Pb}^{2+}$  ions. The increased activate sites helps the enhanced  $\text{Pb}^{2+}$  adsorption.

### 3.3 | $\text{Pb}^{2+}$ adsorption kinetics

It is known that the surface characteristics of the adsorbent are key factors influencing the adsorption rate, and the diffusion resistance significantly influences the ion transfer.<sup>[33]</sup> To better understand the changes in the metal ion adsorption amount related to time progression, we studied the adsorption kinetics using several kinetic models.

The pseudo-first-order kinetic equation is expressed as a linear equation:<sup>[30,33]</sup>

$$\lg(q_e - q_t) = \lg q_e - \frac{k_1}{2.303} t \quad (12)$$

Here,  $q_e$  and  $q_t$  are the adsorbed  $\text{Pb}^{2+}$  (mg/g) at equilibrium and time  $t$ , respectively, and  $k_1$  is the pseudo-first-order kinetic rate constant (/min). When we apply the initial phase (0.5–10 min) data into the pseudo-first-order kinetic model, we can obtain a near-straight line. We then compare the calculated  $q_e$  with the experimental data, plotting  $\lg(q_e - q_t)$  against  $t$  (Figure 6a). Using linear regression to obtain the slope and intercept of the straight line, the pseudo-first-order kinetic rate constant  $k_1$  and

the theoretical  $\text{Pb}^{2+}$  equilibrium adsorption amount  $q_{e,\text{cal}}$  can be calculated. From Table 3, the linear regression demonstrates a weak correlation coefficient. The deviation between  $q_{e,\text{cal}}$  and  $q_{e,\text{exp}}$  is large and without an obvious trend. Therefore, we conclude that the  $\text{Pb}^{2+}$  adsorption in PAA/alumina composites does not follow the pseudo-first-order kinetics.

The pseudo-second-order kinetic equation takes the following form:<sup>[30,33]</sup>

$$\frac{t}{q_t} = \frac{1}{k_2 q_e^2} + \frac{1}{q_e} t \quad (13)$$

Here,  $q_e$  and  $q_t$  take the same meaning as in Equation (12), while  $k_2$  is the pseudo-second-order kinetic rate constant ( $\text{g mg}^{-1} \text{min}^{-1}$ ). Plotting  $t/q_t$  against  $t$  affords a straight line (Figure 6b). After fitting with linear regression to obtain the slope and intercept, the pseudo-second-order kinetic rate constant  $k_2$  and the theoretical  $\text{Pb}^{2+}$  equilibrium adsorption amount  $q_{e,\text{cal}}$  can be calculated. From Table 3, the pseudo-second-order model demonstrates a strong correlation, and the deviation between  $q_{e,\text{cal}}$  and  $q_{e,\text{exp}}$  is much smaller than that obtained using the pseudo-first-order model. Therefore, the  $\text{Pb}^{2+}$  adsorption in PAA/alumina nanocomposites likely follows the pseudo-second-order kinetic model.

However, the pseudo-second-order model cannot specify the detailed mechanism of the ion adsorption process. The adsorption process in porous media can be separated into three stages.<sup>[34]</sup> The first stage is the exterior-particle diffusion while the adsorbate moves from solution to the surface of the adsorbent. Followed is the intra-particle diffusion in

**TABLE 3** Parameters calculated from different kinetic models of  $\text{Pb}^{2+}$  adsorption in alumina and PAA/alumina composites

|                                     | $q_{e,\text{exp}}$ (mg/g) | Parameters of pseudo-first-order kinetic model       |              |       |
|-------------------------------------|---------------------------|--|--------------|-------|
|                                     |                           | $q_{e,\text{cal}}$ (mg/g)                            | $k_1$ (/min) | $R^2$ |
| $\text{Al}_2\text{O}_3$             | 33.51                     | 20.00  | 0.130        | .959  |
| $\text{P}_{10,\text{in}}/\text{Al}$ | 32.75                     | 6.85   | 0.141        | .843  |
| $\text{P}_{90,\text{in}}/\text{Al}$ | 34.27                     | 16.73  | 0.085        | .904  |
|                                     | $q_{e,\text{cal}}$ (mg/g) | Parameters of pseudo-second-order kinetic model      |              |       |
|                                     |                           | $k_2$ (g/(mg min))                                   | $R^2$        |       |
| $\text{Al}_2\text{O}_3$             | 29.67                     | 0.070  | .999         |       |
| $\text{P}_{10,\text{in}}/\text{Al}$ | 28.41                     | 0.059  | .999         |       |
| $\text{P}_{90,\text{in}}/\text{Al}$ | 31.53                     | 0.215  | .999         |       |
|                                     | $C$ (mg/g)                | Parameters of intra-particle diffusion kinetic model |              |       |
|                                     |                           | $k_i$ (mg/(g min <sup>1/2</sup> ))                   | $R^2$        |       |
| $\text{Al}_2\text{O}_3$             | 10.83                     | 6.99   | .950         |       |
| $\text{P}_{10,\text{in}}/\text{Al}$ | 6.99                      | 7.67   | .971         |       |
| $\text{P}_{90,\text{in}}/\text{Al}$ | 25.37                     | 2.26   | .890         |       |

which the adsorbate diffuses inside the adsorbent pores. The last stage is the interaction between the adsorbate and the active sites of the adsorbent and is usually so fast to be omitted. The intra-particle diffusion model is introduced to provide a more detailed description of the  $\text{Pb}^{2+}$  adsorption in PAA/alumina nanocomposites. When using this model, the exterior-particle diffusion is omitted, so the intra-particle diffusion is the only rate-limiting step. This assumption is valid for most solutions. The expression of the intra-particle diffusion model is as follows:<sup>[30,34]</sup>

$$q_t = k_i t^{1/2} + C \quad (14)$$

Here,  $q_t$  has the same meaning as in Equation (12),  $k_i$  is the intra-particle diffusion rate constant ( $\text{mg g}^{-1} \text{min}^{-1/2}$ ), and  $C$  ( $\text{mg/g}$ ) is a constant related to the intra-particle diffusion.

Plotting  $q_t$  against  $t^{1/2}$  affords a diagram in which the initial phase appears as a straight line (Figure 6c). The diagrams in the figure appear to fall into two near-linear sections, a fast-rising intra-particle diffusion phase followed by a stagnant equilibrium phase. After fitting with linear regression to obtain the slope and intercept,  $k_i$  and  $C$  can be calculated (Table 3).  $C$  represents the effects of the boundary layer (the exterior liquid phase thin layer) which can introduce considerable influence on ion diffusion rates.<sup>[35]</sup> In Table 3, the  $C$  values are not near zero, indicating the blockage of the pores renders the intra-particle diffusion not the only rate-limiting stage. Among the two nanocomposite samples studied here,  $\text{P}_{90,\text{in}}/\text{Al}$  has a higher  $C$  value and a smaller  $k_i$  value than  $\text{P}_{10,\text{in}}/\text{Al}$ . Therefore, the former sample has pores more clogged than the latter, causing other factors than intra-particle diffusion to become rate-limiting.

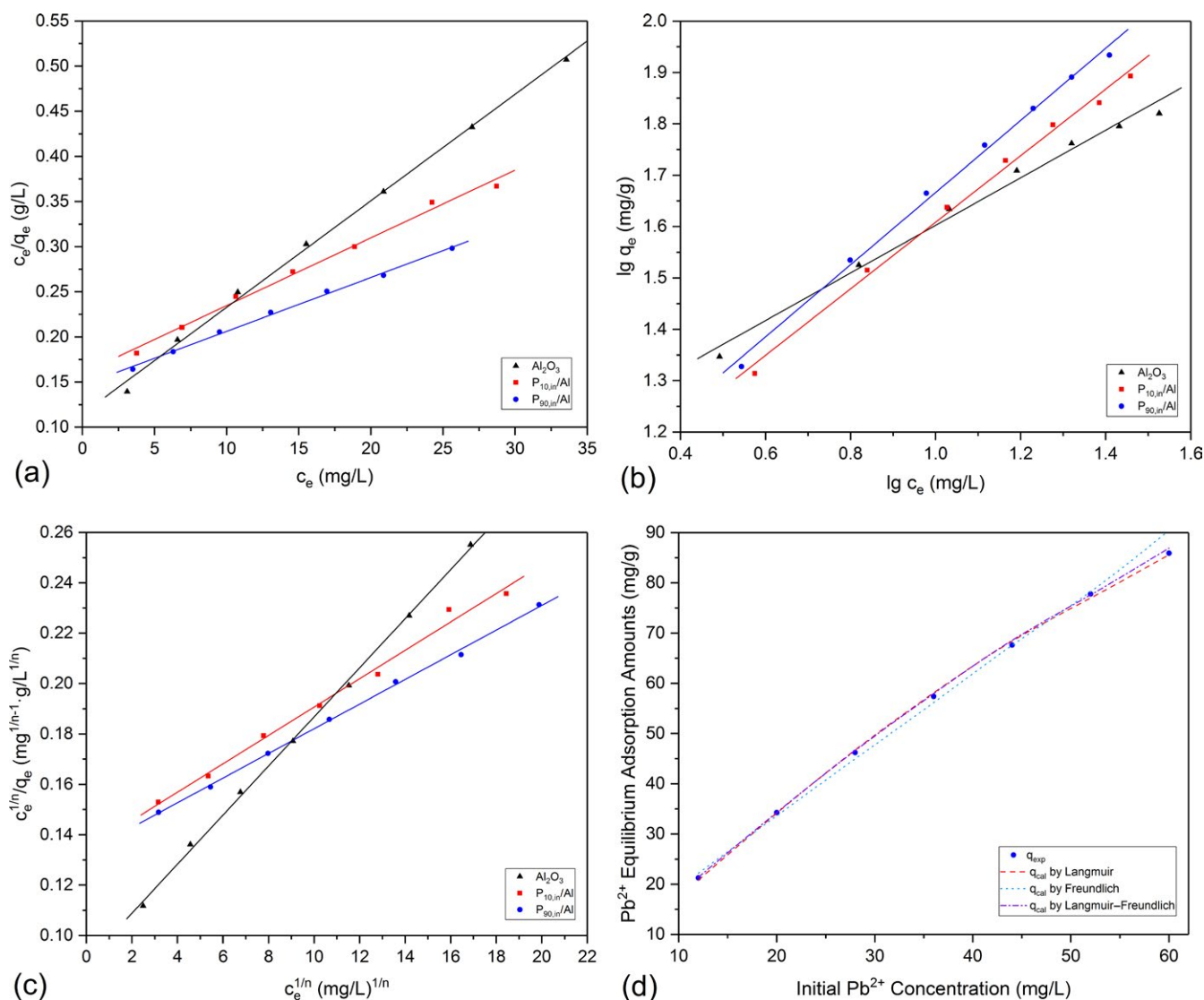


**FIGURE 7** Fitted plots of (a) the Langmuir isotherm, (b) the Freundlich isotherm, and (c) the Langmuir–Freundlich isotherm model of  $\text{Pb}^{2+}$  adsorption in alumina and PAA/alumina composites; (d) comparison between calculated values via different adsorption isotherm models and experimental values

**TABLE 4** Calculated parameters of  $\text{Pb}^{2+}$  adsorption in alumina and PAA/alumina composites from the Langmuir, Freundlich, and Langmuir–Freundlich isotherms

|                                     | $q_{\max}$ (mg/g) | $K_L \times 10^3$ (L/mg) | $R_L$ | $K_F$ (mg/g) | $n$  | $R^2$ | $\chi^2$ |
|-------------------------------------|-------------------|--------------------------|-------|--------------|------|-------|----------|
| Langmuir model                      |                   |                          |       |              |      |       |          |
| $\text{Al}_2\text{O}_3$             | 84.74             | 102.63                   | 0.619 |              |      | .997  | 0.229    |
| $\text{P}_{10,\text{in}}/\text{Al}$ | 133.16            | 47.01                    | 0.262 |              |      | .992  | 0.122    |
| $\text{P}_{90,\text{in}}/\text{Al}$ | 167.79            | 40.63                    | 0.291 |              |      | .996  | 0.042    |
| Freundlich model                    |                   |                          |       |              |      |       |          |
| $\text{Al}_2\text{O}_3$             |                   |                          |       | 13.78        | 2.16 | .987  | 0.498    |
| $\text{P}_{10,\text{in}}/\text{Al}$ |                   |                          |       | 9.14         | 1.54 | .994  | 0.364    |
| $\text{P}_{90,\text{in}}/\text{Al}$ |                   |                          |       | 9.21         | 1.42 | .995  | 0.341    |
| Langmuir–Freundlich model           |                   |                          |       |              |      |       |          |
| $\text{Al}_2\text{O}_3$             | 103.13            | 107.86                   |       |              | 1.24 | .991  | 0.034    |
| $\text{P}_{10,\text{in}}/\text{Al}$ | 177.06            | 42.10                    |       |              | 1.15 | .998  | 0.066    |
| $\text{P}_{90,\text{in}}/\text{Al}$ | 204.36            | 36.74                    |       |              | 1.08 | .998  | 0.036    |

Comparing the three kinetic models, the pseudo-second-order model best describes the metal ion adsorption process in the PAA/alumina nanocomposites. When discussing the  $k_2$  values,  $\text{P}_{90,\text{in}}/\text{Al}$  has a faster adsorption rate than  $\text{P}_{10,\text{in}}/\text{Al}$ . In these nanocomposites, the adsorption sites are primarily provided by PAA in the form of carboxylate groups. In  $\text{P}_{10,\text{in}}/\text{Al}$ , most PAA is located inside the alumina pores, while the polymers are located both inside and outside the metal oxide pores in  $\text{P}_{90,\text{in}}/\text{Al}$ . The  $\text{Pb}^{2+}$  ion diffusion inside the pores is more impeded to result in a slow adsorption rate. We also compare the pseudo-second-order  $\text{Pb}^{2+}$  adsorption rate constant  $k_2$  calculated here with that of the PAA/alumina composites prepared via the impregnation method (P. Zhou, Y.-P. Wang, S.-Z.

Luo, B. Wang, P. Bernazzani, T. M. Nguyen, unpublished data). The  $k_2$  values of the nanocomposites reported here are about 4–5 times larger than those reported in a previous work (P. Zhou, Y.-P. Wang, S.-Z. Luo, B. Wang, P. Bernazzani, T. M. Nguyen, unpublished data). We attribute the sluggish metal ion adsorption kinetics in the impregnation samples to the blockage effects brought about by the infiltrated PAA molecules. In situ polymerization appears to afford PAA/alumina with more open pores for metal ion diffusion.

### 3.4 | $\text{Pb}^{2+}$ adsorption isotherms

Adsorption equilibrium can be described by the isothermal equations. In the isothermal equations, the parameters depict the surface characteristics of the adsorbent surface and the adsorption properties under certain temperature and pH. An isothermal diagram reveals the relationship between the adsorption amount of the adsorbate and the adsorbate concentration in solution under equilibrium.<sup>[33]</sup> In this study, we use the parameters obtained by fitting several common adsorption equations to explore the characteristics of the PAA/alumina nanocomposites.

The Langmuir adsorption model has been widely applied to simulate the monolayer adsorption on the adsorbent surface. In this model, the adsorbent surface is assumed to be uniform, and active sites are evenly distributed in the adsorbent.<sup>[36]</sup> The interaction of metal ions with the active sites on the adsorbent surface is not influenced by whether the neighboring sites are occupied.<sup>[34]</sup> The linear form of the Langmuir equation is given as:<sup>[30,32]</sup>

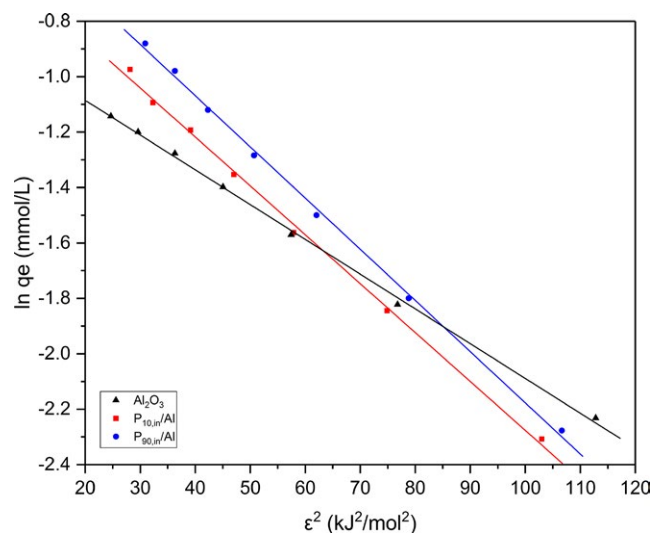


**FIGURE 8** Fitted plot of the Dubinin–Radushkevich isotherm model of  $\text{Pb}^{2+}$  adsorption in alumina and PAA/alumina composites

$$\frac{c_e}{q_e} = \frac{1}{q_{\max}} c_e + \frac{1}{q_{\max} K_L} \quad (15)$$

Here,  $c_e$  is the  $\text{Pb}^{2+}$  concentration (mg/L) in solution at equilibrium,  $q_e$  is the adsorbed  $\text{Pb}^{2+}$  amount by unit mass of adsorbent (mg/g),  $q_{\max}$  is the maximum single-layer  $\text{Pb}^{2+}$  adsorption amount (mg/g), and  $K_L \propto e^{-\Delta G/RT}$  is a constant related to the adsorption free energy (L/mg). Plotting  $c_e/q_e$  against  $c_e$  can produce a diagram (Figure 7a) that is used to generate parameters for linear simulation. From Figure 7a, the slopes and intercepts of the lines can be used to calculate  $q_{\max}$  and  $K_L$ , and the values are listed in Table 4. The linear regression equations produce correlation coefficients greater than 0.99. This shows that the adsorption process is a reasonable chemisorption.  $\text{P}_{90,\text{in}}/\text{Al}$  has the greatest  $q_{\max}$  value, while alumina has the smallest. Both composite samples have a higher  $\text{Pb}^{2+}$  capability than pristine alumina. The equilibrium constant  $R_L$  of the Langmuir adsorption model can also be obtained using the following equation.<sup>[30,33]</sup>

$$R_L = \frac{1}{1 + K_L c_{0,\max}} \quad (16)$$

Here,  $c_{0,\max}$  is the maximum  $\text{Pb}^{2+}$  concentration (mg/L) used in the adsorption experiments.  $R_L$  can be used to interpret the adsorption type. When  $R_L = 0$ , the adsorption process is irreversible. When  $0 < R_L < 1$ , the adsorption is favorable. When  $R_L = 1$ , the adsorption is linear, and when  $R_L > 1$ , the adsorption is disfavored. The  $R_L$  values are shown in Table 4 as well. All values are in between 0 and 1, indicating the  $\text{Pb}^{2+}$  adsorption in both PAA/alumina composites is favorable.

Freundlich adsorption model is used to simulate the multilayer adsorption on the adsorbent surface.<sup>[32]</sup> In this model, it is assumed the adsorbent surface is not even, the adsorbed molecules can interact with each, and multilayer adsorption is possible. The linear equation of the Freundlich model is as follows:<sup>[30,33]</sup>

$$\lg q_e = \frac{1}{n} \lg c_e + \lg K_F \quad (17)$$

Here,  $c_e$  and  $q_e$  take the same meaning as in Equation (15),  $K_f$  is a constant related to adsorbed amount (mg/g), and  $n$  describes the dispersion degree of the active sites. When  $1 < n < 10$ , the adsorption is favorable.<sup>[30]</sup> High  $n$  values represent a relatively evenly distributed adsorbent surface, while

**TABLE 5** Calculated Dubinin–Radushkevich isotherm parameters of  $\text{Pb}^{2+}$  adsorption in alumina and PAA/alumina composites

|                                     | $q_{\text{DR}}$ (mmol/g) | $\lambda$ (mol <sup>2</sup> /kJ <sup>2</sup> ) | $E$ (kJ/mol) | $R^2$ |
|-------------------------------------|--------------------------|--|--------------|-------|
| $\text{Al}_2\text{O}_3$             | 0.434                    | -0.0126  | 6.31         | .998  |
| $\text{P}_{10,\text{in}}/\text{Al}$ | 0.599                    | -0.0177  | 5.32         | .997  |
| $\text{P}_{90,\text{in}}/\text{Al}$ | 0.719                    | -0.0185  | 5.20         | .998  |

low  $n$  values indicate considerable adsorption under low adsorbate concentrations.<sup>[32]</sup> Plotting  $\lg q_e$  against  $\lg c_e$  presents straight lines (Figure 7b). Applying linear regression to the slopes and intercepts,  $K_f$  and  $n$  can be calculated (Table 4). It can be seen that the correlation coefficients are above 0.98, representing a fairly good fitting of the Freundlich model. The  $n$  values are greater than 1, indicating a favorable  $\text{Pb}^{2+}$  adsorption.<sup>[30]</sup> The  $n$  value of  $\text{P}_{90,\text{in}}/\text{Al}$  is lower than that of  $\text{P}_{10,\text{in}}/\text{Al}$ , indicating the higher  $\text{Pb}^{2+}$  adsorption in  $\text{P}_{90,\text{in}}/\text{Al}$ .

Modifying the Langmuir model with the power law, the Langmuir–Freundlich model was introduced.<sup>[37]</sup> The equation takes the following form:<sup>[32,37]</sup>

$$q_e = \frac{q_{\max} K_L c_e^{1/n}}{1 + K_L c_e^{1/n}} \quad (18)$$

Here,  $n$  takes the same meaning as in the Freundlich model, while the other parameters are the same as in the Langmuir model. After linear regression operation,  $q_{\max}$ ,  $K_L$ , and  $n$  can be solved. Plotting  $c_e^{1/n}/q_e$  against  $c_e^{1/n}$  produces straight lines (Figure 7c). The calculated parameters are listed in Table 4. The results of the Langmuir–Freundlich model are similar to those of the Langmuir and Freundlich models. The  $\text{Pb}^{2+}$  adsorption amount is more in  $\text{P}_{90,\text{in}}/\text{Al}$  than in  $\text{P}_{10,\text{in}}/\text{Al}$ , while that in the two composite samples is higher than in pristine alumina.

The above three models all provide reasonably high correlation coefficient values in describing the  $\text{Pb}^{2+}$  adsorption. We apply the  $\chi^2$  test to analyze the simulation results of the three models. The equation of the test is as follows:<sup>[29,38]</sup>

$$\chi^2 = \sum \frac{(q_{\text{exp}} - q_{\text{cal}})^2}{q_{\text{cal}}} \quad (19)$$

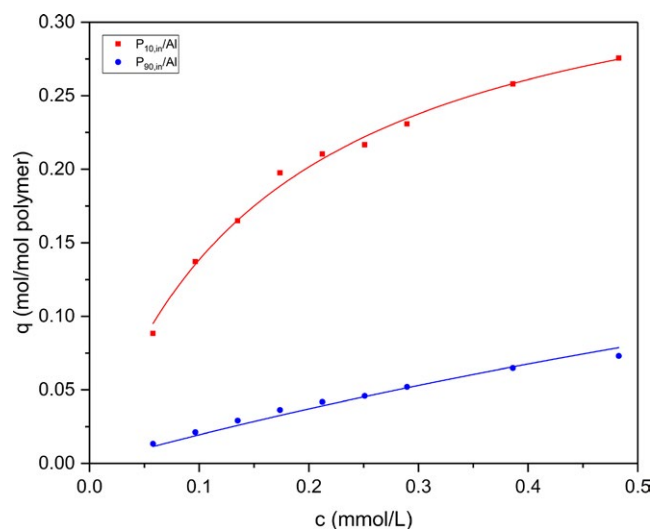


**FIGURE 9** Complexation equilibrium curves of  $\text{Pb}^{2+}$  to PAA in PAA/alumina composites

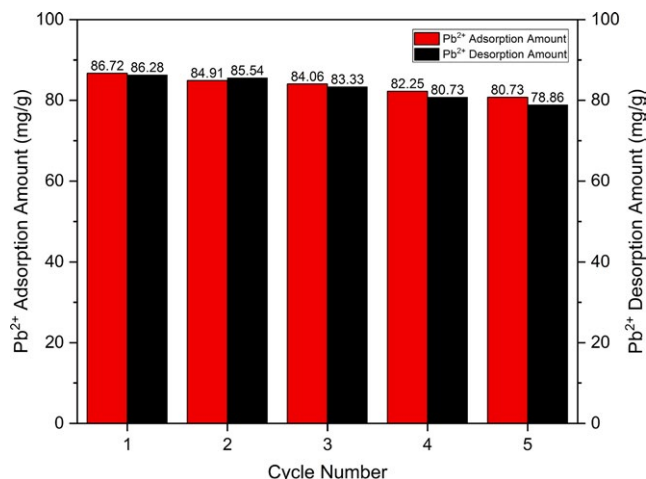


**FIGURE 10** Desorption and regeneration ability of P<sub>90,in</sub>/Al

**TABLE 6** PAA–Pb<sup>2+</sup> stability constants, equilibrium constants, and complexation constants measured at different pH values

|                        | lg <i>b</i> <sub>1</sub> | lg <i>b</i> <sub>2</sub> | lg <i>b</i> <sub>3</sub> | lg <i>k</i> <sub>3</sub> | <i>n</i> | <i>R</i> <sup>2</sup> |
|------------------------|--------------------------|--------------------------|--------------------------|--------------------------|----------|-----------------------|
| PAA <sup>a</sup>       | −1.10                    | −0.20                    | −1.30                    | 0.00                     | –        | –                     |
| P <sub>10,in</sub> /Al | −6.48                    | −0.27                    | −6.75                    | 4.27                     | 0.77     | .989                  |
| P <sub>90,in</sub> /Al | −9.34                    | −0.57                    | −9.90                    | 4.40                     | 0.60     | .964                  |

<sup>a</sup>Data were obtained from reference<sup>[19]</sup>.

Here,  $q_{\text{exp}}$  is the experimental Pb<sup>2+</sup> adsorption amount at equilibrium (mg/g), and  $q_{\text{cal}}$  is the calculated Pb<sup>2+</sup> adsorption amount at equilibrium (mg/g) using different models at established initial Pb<sup>2+</sup> concentrations.  $\chi^2$  describes the deviation between the experimental result and the calculated value for each adsorption isotherm model. Smaller  $\chi^2$  values demonstrate that the simulation results better fit the experimental data.<sup>[30,38]</sup> Figure 7d illustrates the  $\chi^2$  test results. From the figure, the Langmuir model better describes the Pb<sup>2+</sup> adsorption in PAA/alumina composites than does the Freundlich model. We can construe that under the experimental conditions, Pb<sup>2+</sup> adsorption in PAA/alumina composites is primarily monolayer. At higher Pb<sup>2+</sup> concentrations, the Langmuir model results deviate from the experimental results. The Langmuir–Freundlich model can best interpret the adsorption results within the full concentration range.

The average adsorption free energy  $E$  describes the free energy change when moving 1 mol Pb<sup>2+</sup> ions in solution from infinity to the adsorbent surface. The value is obtained using the following equation:<sup>[30,33]</sup>

$$E = \frac{1}{\sqrt{-2\lambda}} \quad (20)$$

Constant  $\lambda$  (mol<sup>2</sup>/kJ<sup>2</sup>) can be obtained by applying the Dubinin–Radushkevich model, which illustrates adsorption properties.<sup>[33]</sup> The Dubinin–Radushkevich model is defined as follows:<sup>[30,33]</sup>

$$\ln q_e = \ln q_{\text{DR}} - \lambda \varepsilon^2 \quad (21)$$

Here,  $q_e$  and  $q_{\text{DR}}$  are the equilibrium and maximum Pb<sup>2+</sup> amounts (mmol/g), respectively, and  $\varepsilon$  is the Polanyi adsorption potential (kJ/mol) which is calculated through using the following equation:<sup>[30,33]</sup>

$$\varepsilon = RT \ln \left( 1 + \frac{1}{c_e} \right) \quad (22)$$

$R$  is the gas constant (kJ mol<sup>−1</sup> K<sup>−1</sup>),  $T$  is the temperature (K), and  $c_e$  is the Pb<sup>2+</sup> concentration (mM) in solution at equilibrium. Plotting  $\ln q_e$  against  $\varepsilon^2$  yields straight lines (Figure 8). Linear regression of the curves' slopes and intercepts affords data to be used in the calculation of  $q_{\text{DR}}$  and  $\lambda$  (Table 5). From the table,  $q_{\text{DR}}$  increases with greater adsorbed PAA amount. The result is similar to the results obtained using the other adsorption isotherm models. After acquiring  $q_{\text{DR}}$  and  $\lambda$ , the average adsorption free energy  $E$  values are given in Table 5. The multitude of  $E$  is related to the interaction mechanism. When  $8.0 < E < 16.0$  kJ/mol, the adsorption process follows an ion exchange mechanism. When  $E < 8.0$  kJ/mol, adsorption is primarily a physical process.<sup>[33]</sup> According to Table 5, the Pb<sup>2+</sup> adsorption in PAA/alumina composites appears as a physical one.

The complexation equilibrium of Pb<sup>2+</sup> to PAA can be investigated if the following assumptions are met: The PAA functional groups (−COOH/−COO<sup>−</sup>) occupied by alumina surface sites are negligible and so is the amount of Pb(OH)<sub>2</sub>.<sup>[19]</sup> The Pb<sup>2+</sup> amount  $q$  (mol mol<sup>−1</sup><sub>polym</sub>) complexed with PAA is obtained via the conversion of supernatant Pb<sup>2+</sup> concentration. Plotting  $q$  against the initial Pb<sup>2+</sup> concentration affords the complexation equilibrium diagrams (Figure 9). Usually, there are two or more PAA functional groups complexed with one Pb<sup>2+</sup> ion.<sup>[19]</sup> The calculation of the complexation equilibrium constants is given in the Experiments and Methods section, and the results are listed in Table 6. The complexation constant  $n$  obtained in this study is smaller than that of Pb<sup>2+</sup> complexed with pure PAA presented in reference.<sup>[19]</sup> In the literature,  $n$  is not given a definitive value even though we could extrapolate that to be around 1.5–2.0. This value has been correlated with the complexation type represented as either the bridging bidentate or the chelating bidentate mode; that is, one metal ion is coordinated to two carboxylate groups. Our obtained value is about a half of the reported value. It is interpreted that PAA molecules located inside alumina

pores are restricted to form complexes with  $\text{Pb}^{2+}$ . Thus, the complexation degree in PAA/alumina is lower than that in pure PAA.

### 3.5 | Desorption and regeneration

Practical application of the adsorbent requires excellent regeneration–reuse property.<sup>[39]</sup> Therefore, we examined the desorption and regeneration of  $\text{P}_{90,\text{in}}/\text{Al}$ , and the results are shown in Figure 10. It can be found that the  $\text{Pb}^{2+}$  adsorption capacity of the sample was not much affected, which was still maintained at  $\geq 90\%$  at the fifth cycle. These results indicate that as-prepared PAA/alumina nanocomposites are suitable for efficient removal of  $\text{Pb}^{2+}$  from wastewater.<sup>[40–89]</sup>

## 4 | CONCLUSIONS

Two poly(acrylic acid)/alumina (PAA/alumina) composite materials,  $\text{P}_{10,\text{in}}/\text{Al}$  and  $\text{P}_{90,\text{in}}/\text{Al}$ , were prepared via in situ polymerization after impregnating acrylic acid into mesopores of  $\gamma$ -alumina. The two nanocomposites had  $\sim 1/4$ - and two-monolayer PAA coverage, respectively, as measured by thermogravimetry. Organic component loss was low during Soxhlet extraction, suggesting good stability of the materials. Three kinetic models, pseudo-first-order model, pseudo-second-order model, and intraparticle diffusion model, were performed on the metal ion sorption data, and the results suggest a well-fitted pseudo-second-order kinetics. The Langmuir, Freundlich, Langmuir–Freundlich, and Dubinin–Radushkevich isotherms were also applied to fit the metal ion sorption equilibrium data. The maximum  $\text{Pb}^{2+}$  equilibrium sorption capacity of the two composite samples,  $q_{\text{max}}$ , evaluated by the Langmuir model at  $25^\circ\text{C}$  was 133.16 mg/g and 167.79 mg/g, respectively. The Langmuir–Freundlich model could best interpret the adsorption results at the whole concentration range. The complexation equilibrium constants  $B_2$  and  $n$  were smaller than those of  $\text{Pb}^{2+}$  complexed with pure PAA due to the restriction of the inner pores of alumina.

### ACKNOWLEDGMENT

The authors gratefully acknowledge the financial support from SINOPEC Maoming Company.

### ORCID

Ya-Ping Wang  <http://orcid.org/0000-0002-3308-4728>

Bin Wang  <http://orcid.org/0000-0002-1447-7577>

## REFERENCES

- [1] M. Han, X. Gao, J. Z. Su, S. Nie, *Nat. Biotechnol.* **2001**, *19*(7), 631.
- [2] R. Bleach, B. Karagoz, S. M. Prakash, T. P. Davis, C. Boyer, *ACS Macro Lett.* **2014**, *3*, 591.
- [3] I. V. Kityk, J. Ebothé, I. Fuks-Janczarek, A. A. Umar, K. Kobayashi, M. Oyama, B. Sahraoui, *Nanotechnology* **2005**, *16*, 1687.
- [4] L. R. Hirsch, R. J. Stafford, J. A. Bankson, S. R. Sershen, B. Rivera, R. E. Price, J. D. Hazle, N. J. Halas, J. L. West, *Proc. Natl Acad. Sci.* **2003**, *100*, 13549.
- [5] M. Choi, F. Kleitz, D. Liu, H. Y. Lee, W.-S. Ahn, R. Ryoo, *J. Am. Chem. Soc.* **2005**, *127*, 1924.
- [6] M. Mizuno, M. Takahashi, Y. Tokuda, T. Yoko, *Chem. Mater.* **2006**, *18*, 2075.
- [7] S. M. Grant, S. M. Woods, A. Gericke, M. Jaroniec, *ACS Appl. Mater. Interfaces.* **2011**, *3*, 4480.
- [8] G. L. Drisko, P. Imperia, M. de los Reyes, V. Luca, R. A. Caruso, *Langmuir* **2010**, *26*, 14203.
- [9] X. Zhang, G. J. Blanchard, *ACS Appl. Mater. Interfaces.* **2015**, *7*, 6054.
- [10] K. Mylvaganam, L. Zhang, *J. Phys. Chem. C* **2013**, *117*, 2817.
- [11] Y. Zheng, J. Zhang, A. Wang, *Chem. Eng. J.* **2009**, *155*(1–2), 215.
- [12] L. Jiang, P. Liu, S. Zhao, *Colloids Surf. Physicochem. Eng. Asp.* **2015**, *470*, 31.
- [13] L. Zhou, C. Shang, Z. Liu, G. Huang, A. A. Adesina, *J. Colloid Interface Sci.* **2012**, *366*(1), 165.
- [14] Q. Fang, S. Duan, J. Zhang, J. Li, K. C.-F. Leung, *J. Mater. Chem. A* **2017**, *5*, 2947.
- [15] L. Liu, S.-Z. Luo, B. Wang, Z. Guo, *Appl. Surf. Sci.* **2015**, *345*, 116.
- [16] B. Wang, Y.-P. Wang, P. Zhou, Z.-Q. Liu, S.-Z. Luo, W. Chu, Z. Guo, *Colloids Surf. Physicochem. Eng. Asp.* **2017**, *514*, 168.
- [17] J. S. Noh, J. A. Schwarz, *J. Colloid Interface Sci.* **1989**, *130*(1), 157.
- [18] K. Bourikas, J. Vakros, C. Kordulis, A. Lycourghiotis, *J. Phys. Chem. B* **2003**, *107*, 9441.
- [19] T. Tomida, K. Hamaguchi, S. Tunashima, M. Katoh, S. Masuda, *Ind. Eng. Chem. Res.* **2001**, *40*, 3557.
- [20] J. Choi, M. F. Rubner, *Macromolecules* **2005**, *38*(1), 116.
- [21] B. N. Dickhaus, R. Priefer, *Colloids Surf. Physicochem. Eng. Asp.* **2016**, *488*, 15.
- [22] R. M. Florou, A. P. Davis, A. Torrents, *Environ. Sci. Technol.* **2001**, *35*, 348.
- [23] H. R. Rafiei, M. Shirvani, O. A. Ogunseitan, *Appl. Water Sci.* **2016**, *6*(4), 331.
- [24] Y. Wang, F. M. Michel, C. Levard, Y. Choi, P. J. Eng, G. E. Brown, *Environ. Sci. Technol.* **2013**, *47*, 12131.
- [25] C. F. Conrad, C. J. Chisholm-Brause, M. J. Kelley, *J. Colloid Interface Sci.* **2002**, *248*(2), 275.
- [26] A. Shokati Poursani, A. Nilchi, A. H. Hassani, M. Shariat, J. Nouri, *Int. J. Environ. Sci. Technol.* **2015**, *12*, 2003.
- [27] E. K. Yetimoğlu, M. Fırlak, M. V. Kahraman, S. Deniz, *Polym. Adv. Technol.* **2011**, *22*(5), 612.
- [28] D. G. Strawn, A. M. Scheidegger, D. L. Sparks, *Environ. Sci. Technol.* **1998**, *32*, 2596.
- [29] C. H. Campos, C. C. Torres, B. F. Urbano, B. L. Rivas, *Polym. Int.* **2015**, *64*(5), 595.
- [30] T. K. Naiya, A. K. Bhattacharya, S. K. Das, *J. Colloid Interface Sci.* **2009**, *333*(1), 14.
- [31] H. Chen, D. Shao, J. Li, X. Wang, *Chem. Eng. J.* **2014**, *254*, 623.

- [32] M. Boroumand Jazi, M. Arshadi, M. J. Amiri, A. Gil, *J. Colloid Interface Sci.* **2014**, 422, 16.
- [33] A. M. El-Kamash, *J. Hazard. Mater.* **2008**, 151(2–3), 432.
- [34] Q. Yu, R. Zhang, S. Deng, J. Huang, G. Yu, *Water Res.* **2009**, 43, 1150.
- [35] H. Ge, X. Fan, *Chem. Eng. Technol.* **2011**, 34(10), 1745.
- [36] Y. J. O. Asencios, M. R. Sun-Kou, *Appl. Surf. Sci.* **2012**, 258, 10002.
- [37] S. Bailliez, A. Nzihou, E. Bèche, G. Flamant, *Process Saf. Environ. Prot.* **2004**, 82(2), 175.
- [38] J. Zhang, A. Wang, *J. Chem. Eng. Data* **2010**, 55, 2379.
- [39] D. Shao, G. Hou, J. Li, T. Wen, X. Ren, X. Wang, *Chem. Eng. J.* **2014**, 255, 604.
- [40] H. Gu, C. Liu, J. Zhu, J. Gu, E. K. Wujcik, L. Shao, N. Wang, H. Wei, R. Scaffaro, J. Zhang, Z. Guo, *Adv. Compos. Hybrid Mater.* **2018**, 1, 1.
- [41] T. Su, Q. Shao, Z. Qin, Z. Guo, Z. Wu, *ACS Catal.* **2018**, 8, 2253.
- [42] W. Yang, X.-L. Wang, J. Li, X. Yan, S. Ge, S. Tadakamalla, Z. Guo, *Polym. Eng. Sci.* <https://doi.org/10.1002/pen.24675>.
- [43] C. Wang, B. Mo, Z. He, X. Xie, C. X. Zhao, L. Zhang, Q. Shao, X. Guo, E. K. Wujcik, Z. Guo, *Polymer* **2018**, 138, 363.
- [44] X. Cui, G. Zhu, Y. Pan, Q. Shao, C. X. Zhao, M. Dong, Y. Zhang, Z. Guo, *Polymer* **2018**, 138, 203.
- [45] J. Lin, X. Chen, C. Chen, J. Hu, C. Zhou, X. Cai, W. Wang, C. Zheng, P. Zhang, J. Cheng, Z. Guo, H. Liu, *ACS Appl. Mater. Interfaces.* **2018**, 10, 6124.
- [46] C. Wang, Z. He, X. Xie, X. Mai, Y. Li, T. Li, M. Zhao, C. Yan, H. Liu, E. K. Wujcik, Z. Guo, *Macromol. Mater. Eng.* **2018**, 303, 1700462.
- [47] Q. Hou, J. Ren, H. Chen, P. Yang, Q. Shao, M. Zhao, X. Zhao, H. He, N. Wang, Q. Luo, Z. Guo, *ChemElectroChem* **2018**, 5, 725.
- [48] Y. Li, B. Zhou, G. Zheng, X. Liu, T. Li, C. Yan, C. Cheng, K. Dai, C. Liu, C. Shen, Z. Guo, *J. Mater. Chem. C* **2018**, 6, 2258.
- [49] P. Zhou, S. Wang, C. Tao, X. Guo, L. Hao, Q. Shao, L. Liu, Y.-P. Wang, W. Chu, B. Wang, S.-Z. Luo, Z. Guo, *Adv. Polym. Technol.* <https://doi.org/10.1002/adv.21908>.
- [50] X. Q. Cheng, Z. X. Wang, X. Jiang, T. Li, C. H. Lau, Z. Guo, J. Ma, L. Shao, *Progress Mater. Sci.* **2018**, 92, 258.
- [51] C. Wang, Y. Wu, Y. Li, Q. Shao, X. Yan, C. Han, Z. Wang, Z. Liu, Z. Guo, *Polym. Adv. Technol.* **2018**, 29, 668.
- [52] C. Lin, L. Hu, C. Cheng, K. Sun, X. Guo, Q. Shao, J. Li, N. Wang, Z. Guo, *Electrochim. Acta* **2018**, 260, 65.
- [53] Y. He, S. Yang, H. Liu, Q. Shao, Q. Chen, C. Lu, Y. Jiang, C. Liu, Z. Guo, *J. Colloid Interf. Sci.* **2018**, 517, 40.
- [54] M. Zhao, L. Meng, L. Ma, L. Ma, X. Yang, Y. Huang, J. E. Ryu, A. Shankar, T. Li, C. Yan, Z. Guo, *Compos. Sci. Technol.* **2018**, 154, 28.
- [55] X. Wang, X. Liu, H. Yuan, H. Liu, C. Liu, T. Li, C. Yan, X. Yan, C. Shen, Z. Guo, *Mater. Design* **2018**, 139, 372.
- [56] T. Liu, K. Yu, L. Gao, H. Chen, N. Wang, L. Hao, T. Li, H. He, Z. Guo, *J. Mater. Chem. A* **2017**, 5, 17848.
- [57] Z. Sun, L. Zhang, F. Dang, Y. Liu, Z. Fei, Q. Shao, H. Lin, J. Guo, L. Xiang, N. Yerrad, Z. Guo, *CrystEngComm* **2017**, 19, 3288.
- [58] L. Zhang, M. Qin, W. Yu, Q. Zhang, H. Xie, Z. Sun, Q. Shao, X. Guo, L. Hao, Y. Zheng, Z. Guo, *J. Electrochem. Soc.* **2017**, 164, H1086.
- [59] L. Zhang, W. Yu, C. Han, J. Guo, Q. Zhang, H. Xie, Q. Shao, Z. Sun, Z. Guo, *J. Electrochem. Soc.* **2017**, 164, H651.
- [60] B. Song, T. Wang, H. Sun, Q. Shao, J. Zhao, K. Song, L. Hao, L. Wang, Z. Guo, *Dalton Trans.* **2017**, 46, 15769.
- [61] X. Lou, C. Lin, Q. Luo, J. Zhao, B. Wang, J. Li, Q. Shao, X. Guo, N. Wang, Z. Guo, *ChemElectroChem.* **2017**, 4, 3171.
- [62] K. Zhang, G.-H. Li, L.-M. Feng, N. Wang, J. Guo, K. Sun, K.-X. Yu, J.-B. Zeng, T. Li, Z. Guo, M. Wang, *J. Mater. Chem. C* **2017**, 5, 9359.
- [63] C. Hu, Z. Li, Y. Wang, J. Gao, K. Dai, G. Zheng, C. Liu, C. Shen, H. Song, Z. Guo, *J. Mater. Chem. C* **2017**, 5, 2318.
- [64] H. Liu, M. Dong, W. Huang, J. Gao, K. Dai, J. Guo, G. Zheng, C. Liu, C. Shen, Z. Guo, *J. Mater. Chem. C* **2017**, 5, 73.
- [65] J. Zhao, L. Wu, C. Zhan, Q. Shao, Z. Guo, L. Zhang, *Polymer* **2017**, 133, 272.
- [66] C. Wang, M. Zhao, J. Li, J. Yu, S. Sun, S. Ge, X. Guo, F. Xie, B. Jiang, E. K. Wujcik, Y. Huang, N. Wang, Z. Guo, *Polymer* **2017**, 131, 263.
- [67] Y. Ma, L. Lv, Y. Guo, Y. Fu, Q. Shao, T. Wu, S. Guo, K. Sun, X. Guo, E. K. Wujcik, Z. Guo, *Polymer* **2017**, 128, 12.
- [68] K. Sun, P. Xie, Z. Wang, T. Su, Q. Shao, J. E. Ryu, X. Zhang, J. G. A. Shankar, J. Li, R. Fan, D. Cao, Z. Guo, *Polymer* **2017**, 125, 50.
- [69] Y. Li, X. Wu, J. Song, J. Li, Q. Shao, N. Cao, N. Lu, Z. Guo, *Polymer* **2017**, 124, 41.
- [70] J. Huang, Y. Cao, Q. Shao, X. Peng, Z. Guo, *Ind. Eng. Chem. Res.* **2017**, 56, 10689.
- [71] C. Cheng, R. Fan, Z. Wang, Q. Shao, X. Guo, P. Xie, Y. Yin, Y. Zhang, L. An, Y. Lei, J. E. Ryu, A. Shankar, Z. Guo, *Carbon* **2017**, 125, 103.
- [72] Y. Zheng, Y. Zheng, S. Yang, Z. Guo, T. Zhang, H. Song, Q. Shao, *Green Chem. Lett. Rev.* **2017**, 10, 202.
- [73] Z. Wu, S. Gao, L. Chen, D. Jiang, Q. Shao, B. Zhang, Z. Zhai, C. Wang, M. Zhao, Y. Ma, X. Zhang, L. Weng, M. Zhang, Z. Guo, *Macromol. Chem. Phys.* **2017**, 218, 1.
- [74] Z. Liu, X. Liu, G. Zheng, K. Dai, C. Liu, C. Shen, R. Yin, Z. Guo, *Polym. Testing* **2017**, 58, 227.
- [75] H. Liu, W. Huang, X. Yang, K. Dai, G. Zheng, C. Liu, C. Shen, X. Yan, J. Guo, Z. Guo, *J. Mater. Chem. C* **2016**, 4, 4459.
- [76] H. Liu, Y. Li, K. Dai, G. Zheng, C. Liu, C. Shen, X. Yan, J. Guo, Z. Guo, *J. Mater. Chem. C* **2016**, 4, 157.
- [77] X. Guan, G. Zheng, K. Dai, C. Liu, X. Yan, C. Shen, Z. Guo, *ACS Appl. Mater. Interfaces.* **2016**, 8, 14150.
- [78] X. Zhu, W. Chen, K. Wu, H. Li, M. Fu, Q. Liu, X. Zhang, *New J. Chem.* **2018**, 42, .
- [79] Z. Hu, D. Zhang, L. Yu, Y. Huang, *J. Mater. Chem. B* **2018**, 6, 518.
- [80] Y. Ding, B. Yang, H. Liu, Z. Liu, X. Zhang, X. Zheng, Q. Liu, *Sensors Actuators B Chem.* **2018**, 259, 775.
- [81] Z. Hu, Q. Shao, M. G. Moloney, X. Xu, D. Zhang, J. Li, C. Zhang, Y. Huang, *Macromolecules* **2017**, 50, 1422.
- [82] Z. Hu, Q. Shao, X. Xu, D. Zhang, Y. Huang, *Compos. Sci. Technol.* **2017**, 142, 294.
- [83] Z. Hu, C. Wang, F. Zhao, X. Xu, S. Wang, L. Yu, D. Zhang, Y. Huang, *Nanoscale* **2017**, 9, 8825.
- [84] Q. Liu, P. Chen, Z. Xu, M. Chen, Y. Ding, K. Yue, J. Xu, *Sensors Actuators B Chem.* **2017**, 251, 339.
- [85] Q. Liu, Y. Yang, X. Lv, Y. Ding, Y. Zhang, J. Jing, C. Xu, *Sensors Actuators B Chem.* **2017**, 240, 726.

- [86] L. Zhang, M. Chen, Y. Jiang, M. Chen, Y. Ding, Q. Liu, *Sensors Actuators B Chem.* **2017**, *239*, 28.
- [87] M. Chen, Y. Ding, Y. Gao, X. Zhu, P. Wang, Z. Shi, Q. Liu, *RSC Adv.* **2017**, *7*, 25220.
- [88] M. Chen, L. Sun, Y. Ding, Z. Shi, Q. Liu, *New J. Chem.* **2017**, *41*, 5853.
- [89] Q. Liu, Y. Yang, H. Li, R. Zhu, Q. Shao, S. Yang, J. Xu, *Biosens. Bioelectron.* **2015**, *64*, 147.

**How to cite this article:** Wang Y-P, Zhou P, Luo S-Z, et al. In situ polymerized poly(acrylic acid)/alumina nanocomposites for Pb<sup>2+</sup> adsorption. *Adv Polym Technol.* 2018;37:2981–2996. <https://doi.org/10.1002/adv.21969>